

# Spontaneous thermal expansion of nematic elastomers

A.R. Tajbakhsh and E.M. Terentjev\*  
Cavendish Laboratory, University of Cambridge  
Madingley Road, Cambridge CB3 0HE, U.K.

November 1, 2018

## Abstract

We study the monodomain (single-crystal) nematic elastomer materials, all side-chain siloxane polymers with the same mesogenic groups and crosslinking density, but differing in the type of crosslinking. Increasing the proportion of long di-functional segments of main-chain nematic polymer, acting as network crosslinking, results in dramatic changes in the uniaxial equilibrium thermal expansion on cooling from isotropic phase. At higher concentration of main chains their behaviour dominates the elastomer properties. At low concentration of main-chain material, we detect two distinct transitions at different temperatures, one attributed to the main-chain, the other to the side-chain component. The effective uniaxial anisotropy of nematic rubber,  $r(T) = \ell_{\parallel}/\ell_{\perp}$  proportional to the effective nematic order parameter  $Q(T)$ , is given by an average of the two components and thus reflects the two-transition nature of thermal expansion. The experimental data is compared with the theoretical model of ideal nematic elastomers; applications in high-amplitude thermal actuators are discussed in the end.

PACS numbers:

61.41.+e Polymers, elastomers, and plastics

61.30.-v Liquid crystals

46.25.Hf Thermoelasticity

---

\*Electronic mail: *emt1000@cam.ac.uk*

# 1 Introduction

Liquid crystalline elastomers (LCE) have attracted a significant experimental and theoretical interest. Recent review articles summarise much of the recent-years research [1, 2, 3, 4, 5]. The novel behavior of these materials arises from a coupling between the liquid crystalline ordering of mesogenic moieties and the elastic properties of the polymer network. Several unusual physical effects have been discovered in LCE: (a) Spontaneous, reversible shape changes on heating or illumination. (b) “Soft elasticity” – mechanical deformation without (or with very low) stress. (c) Mechanical instabilities and discontinuous stress-strain relations on switching of nematic director by mechanical fields [7, 8]. (d) Electrical switching of optical properties with accompanying mechanical strains in [9, 10]. (e) Solid phase nemato-hydrodynamics and unusual rheology and dynamics, leading to anomalous dissipation, mechanical damping and dynamic softness [11, 12].

Theoretical work has been able to develop simple molecular models of ideal nematic network and qualitatively describe or predict nearly all observed phenomena with a description having no free parameters, based only on independently measurable quantities [3]. This theory of an ideal nematic rubber is encompassed in the expression for the free energy density of a nematic rubber in response to a arbitrary general deformation expressed by the strain tensor  $\underline{\underline{\lambda}}$ :

$$F_{\text{elast}} = \frac{1}{2}\mu \text{Tr} \left[ \underline{\underline{\ell}}_0 \cdot \underline{\underline{\lambda}}^T \cdot \underline{\underline{\ell}}^{-1} \cdot \underline{\underline{\lambda}} \right], \quad (1)$$

where  $\mu \approx n_x k_B T$  is the rubber modulus proportional to the crosslinking density of the network. Within the phantom Gaussian chain approximation, the matrix  $\underline{\underline{\ell}}$  (as well as  $\underline{\underline{\ell}}_0$ ) represents the anisotropic distribution of nematic chain segments after the affine deformation  $\underline{\underline{\lambda}}$  is applied (or the initial anisotropy before deformation, in the case of  $\underline{\underline{\ell}}_0$ ). The effective chain anisotropy is the crucial factor in the description. The matrix  $\underline{\underline{\ell}}$  characterises the local nematic director  $\mathbf{n}$  as its principal eigenvector, as well as the degree of local order expressed by the difference between its principal eigenvalues: in the component form  $\ell_{ij} = \ell_{\perp} \delta_{ij} + [\ell_{\parallel} - \ell_{\perp}] n_i n_j$ . Accordingly, the nematic polymer chain has the anisotropic radius of gyration,  $\overline{R}_{\parallel} = (\frac{1}{3} \ell_{\parallel} L)^{1/2}$  and  $\overline{R}_{\perp} = (\frac{1}{3} \ell_{\perp} L)^{1/2}$  for a Gaussian chain of contour length  $L$ . In the isotropic phase both principal values become equal to the single parameter,  $b$ , of chain persistence length:  $\ell_{ij}^{\text{iso}} = b \delta_{ij}$  and  $\overline{R} = (\frac{1}{3} b L)^{1/2}$  along each of the three coordinate axes.

A more recent development allowed to combine the concepts of reptation theory of entangled networks with the anisotropic nature of nematic polymer strands [13], obtaining the “tube model” corrections to the ideal nematic

rubber elastic free energy

$$\begin{aligned}
F_{\text{elast}} = & \frac{2}{3}\mu \frac{2M+1}{3M+1} \text{Tr}(\underline{\underline{\ell}}_0 \cdot \underline{\underline{\lambda}}^T \cdot \underline{\underline{\ell}}^{-1} \cdot \underline{\underline{\lambda}}) \\
& + \frac{3}{2}\mu(M-1) \frac{2M+1}{3M+1} (\langle |\underline{\underline{\ell}}^{-1/2} \cdot \underline{\underline{\lambda}} \cdot \underline{\underline{\ell}}_0^{1/2}| \rangle)^2 \\
& + \mu(M-1) \langle \ln |\underline{\underline{\ell}}^{-1/2} \cdot \underline{\underline{\lambda}} \cdot \underline{\underline{\ell}}_0^{1/2}| \rangle,
\end{aligned} \tag{2}$$

where  $M$  is the average number of entanglements per network strand ( $M = 1$  for an ideal unentangled nematic rubber) and the notation  $\langle \dots \rangle$  stands for an angular averaging of a matrix converted with an arbitrary unit vector [13]. In a real elastomer  $M$  is expected to be rather high since the reptation diffusion and the resulting disentanglement are restricted in a crosslinked network, unlike in the case of uncrosslinked melt where one needs a certain chain length ( $N_e$ ) to form a topological knot [14]. Clearly, at high  $M$  entanglements dominate the rubber modulus, as is indicated by the second and third lines in the Eq. (2). However, it turns out that, although the modified elastic free energy appears different, many key parameters and predictions of the ideal theory remain in force.

One such equilibrium effect stands out in the properties of liquid crystalline elastomers, being especially pronounced when a monodomain (single crystal, permanently aligned [15]) nematic network is prepared. It is the anomalous thermal expansion – the spontaneous elongation of the material along the director axis on cooling from the isotropic phase [16, 17]. It is rather straightforward to derive the equilibrium uniaxial extensional strain by minimisation of the Eq.(1) where the chain anisotropy changes from  $\ell_{\parallel}^{(0)} = \ell_{\perp}^{(0)} = b$ , in the initial state, to a set of values  $\ell_{\parallel} \neq \ell_{\perp}$  with  $\ell_{\parallel}$  along the nematic director  $\mathbf{n}$ , which is also the principal axis of spontaneous extension (see [3] for detail). The result for the uniaxial expansion,

$$\lambda_{\text{th}} = (\ell_{\parallel}/\ell_{\perp})^{1/3}, \tag{3}$$

is a sensitive function of temperature. Remarkably, the same expression for  $\lambda_{\text{th}}$  is obtained from the modified reptation theory of nematic elastomers (2). The reason for this spontaneous uniaxial thermal expansion is the direct coupling between the average chain anisotropy and the nematic order parameter. Depending on this coupling, the magnitude of  $\lambda_{\text{th}}$  could differ greatly (and even change sense from extension to contraction in a polymer with oblate backbone conformation), reaching a maximum in a main-chain nematic polymer systems which could expand, spontaneously and reversibly, by a factor of  $\sim 3 - 4$  [18].

In this paper we focus on the role of the single model parameter in the above molecular theories – the effective chain anisotropy  $\underline{\ell}$ . On the one hand, the strength of the theory is that the effective anisotropy parameter  $r = \ell_{\parallel}/\ell_{\perp}$  could be directly measured by examining the thermal expansion of a uniaxial nematic rubber, cf. Eq.(3), thus leaving no free parameters and allowing quantitative predictions. On the other hand, one appreciates that the value of  $r$  measured in a macroscopic experiment, such as the mechanical deformation, is an effective average parameter of the whole network, not necessarily directly related to the persistent length anisotropy of a particular polymer forming the network.

We examine a sequence of materials, having essentially the same chemical structure and composition of side chain polysiloxane nematic polymer strands but different in the type of permanent chemical crosslinking. Maintaining the constant degree of crosslinking, at 10% (by reacting bonds), we continuously alter the proportion between the two crosslinking agents: (i) flexible di-alkeneoxybenzene units, which are thought to have only a minor effect on the anisotropy of nematic network strands, and (ii) long di-functional chains of main-chain nematic polymer, which create an additional (and very high) anisotropy in the composite material. In all cases we prepare uniformly aligned monodomain nematic networks – single-crystal liquid crystal elastomers (SCLCE) in terminology of [15]. By measuring the spontaneous uniaxial thermal expansion  $\lambda_{\text{th}}$ , we obtain the temperature-dependent effective network anisotropy  $r(T)$ . A parallel thermal study (DSC) identifies the points of nematic phase transitions for all materials and correlates these with the thermo-mechanical response.

We also correlate the thermal expansion (and the effective mechanical anisotropy  $r$ ) with the local nematic order parameter  $Q(T)$ , measured by X-ray diffraction. It is obvious that there has to be a direct relationship, with the limit  $r \rightarrow 1$  at  $Q \rightarrow 0$ . However, the theoretical derivation of such a correspondence is difficult because it is based on the single-chain analysis and is strongly model-dependent, varying from a trivial  $r = (1 + 2Q)/(1 - Q)$  for a freely-jointed chain model to a highly non-linear  $r \sim \exp[3/(1 - Q)]$  in the hairpin regime of main-chain homopolymers [19]. The results show that a linear relationship between  $r(T)$  and  $Q(T)$  holds over a broad range of temperatures.

Finally, we conclude by discussing the possible application of spontaneous deformation of monodomain nematic rubber in thermo-mechanical actuators. Section 4 presents a study of a selected optimised sample, providing the data for deformation under load (the artificial muscle regime [20]) and for the stress-temperature relation at fixed geometry (the dynamic actuator regime). There are competing factors, for instance, the amplitude and the

steepness of the response are in the opposite relation to the response rate. Comparing the materials that span the wide range of possibilities, we propose that highly anisotropic main-chain containing nematic elastomers are most suitable for large-amplitude actuation when the time is a less relevant factor, while the low-anisotropy nematic materials provide the low-amplitude but high-frequency response suitable, for instance, for acoustic applications.

## 2 Experimental

All starting materials and samples of side chain siloxane liquid crystalline elastomers were prepared in the Cavendish Laboratory by modification of the procedure of Finkelmann et al [15, 21]. The polymer backbone was a poly-methylhydrosiloxane with approximately 60 Si-H units per chain, obtained from ACROS Chemicals. The pendant mesogenic groups were 4'-methoxyphenyl-4-(1-buteneoxy) benzoate (MBB), as illustrated in Figure 1, attached to the backbone via the hydrosilation reaction. All networks were chemically crosslinked via the same reaction, in the presence of commercial platinum catalyst COD, obtained from Wacker Chemie, with di-functional crosslinking groups also shown in Fig. 1 (both synthesized in the house). In all cases the crosslinking density was calculated to be 10 mol% of the reacting bonds in the siloxane backbone, so that on average each chain has 9 mesogenic groups between crosslinking sites.

However, the samples were different in the proportion of two crosslinking components. The first crosslinking agent, 1,4 di(11-undecene) benzene (11UB), is a small flexible molecule deemed to have relatively minor effect on the overall mesogenic properties of the liquid crystalline polymer (apart from the trivial effect of added impurity, which is deliberately kept constant in our experiments). The second crosslinking agent was very different: di-vinyl terminated chains  $\alpha$ -{4-[1-(4'-{11-undecenyl}oxy) biphenyl]-2-phenyl] butyl}- $\omega$ -(11-undecenyl) poly-[1-(4-oxydeca methyleneoxy)- biphenyl-2-phenyl] butyl chains that themselves make a main-chain liquid crystal [22]. In our case the crosslinking chains were with  $\sim 74$  rod-like monomers between the terminal vinyl groups (determined by GPC, polydispersity  $\sim 2$ ). Each such long-chain crosslinker connects two siloxane polymer chains.

Calculating the crosslinking density by reacting bonds, as described above, can be quite different from the actual concentration of the species in resulting material. In particular, in the case of MC polymer crosslinker, the relative gram weight of it in the otherwise side-chain polymer matrix is very high: the molecular weight of an average MC crosslinking chain, cf. Fig. 1, is  $34530 \sim 75 \times 456$  – which is much greater than the molecular weight

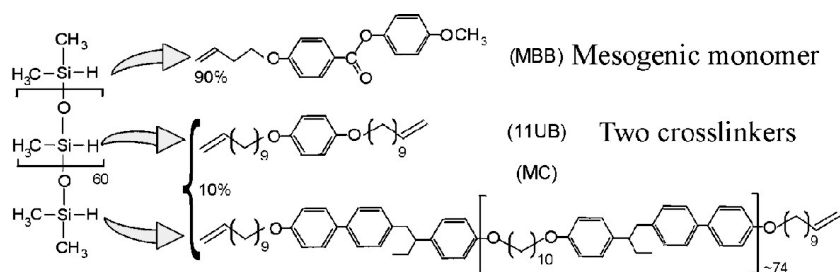


Figure 1: Schematic illustration of the materials used in this work. Siloxane backbone chain with Si-H groups reacting with 90 mol% mesogenic phenylbenzoate side groups (MMB) and 10 mol% of di-vinyl crosslinking groups combining a changing proportion of flexible small-molecule 1,4 alkeneoxybenzene (11UB) and the main-chain nematic polymer of 1-biphenyl-2-phenyl butane (MC).

Samples	%(11UB)	%(MC)	$T_g$ (C)	$T_{ni}$ (C)
MC0	10	0	3	85.5
MC0.1	9.9	0.1	7	85.6(106)
MC0.25	9.75	0.25	2	88(106)
MC0.5	9.5	0.5	7	(91)106
MC1	9	1	2	(98.5)107
MC10	0	10	17	108

Table 1: Proportions of crosslinkers 11UB and MC in the overall crosslinking composition (of 10 mol%) and the corresponding temperatures of glass and nematic-isotropic transitions. Values of  $T_{ni}$  in brackets refer to the second transition observed in “mixed” materials. The glass transition temperature are approximate, with an error of at least  $\pm 5^\circ$ .

of the corresponding 9-unit side-chain polymer strand between crosslinking points ( $2691 \sim 9 \times 299$ ). One may equally regard such a system as a *main-chain nematic rubber network*, end-linked with relatively small crosslinking groups made of side-chain nematic polysiloxane.

The series of materials, synthesized in this way, are referred to by the proportion of MC crosslinker in the total crosslinking composition. In this way, the sample labeled as MC0 is crosslinked purely by the 10 mol% of small-molecule group 11UB. At the opposite end, MC10 refers to the material crosslinked purely by the long main-chain nematic polymer. We find particularly interesting effects occurring at very small proportion of main-chain crosslinker. The borderline case, when the overall mass of MC material in the network composition is approximately equal to that of side-chain polysiloxane, is at approximately 1.75 mol% of MC. We find that compositions close to this are optimal in balancing the increasing amplitude of thermal expansion and the decreasing rate of response. The samples we have studied, MC0.1, MC0.25, MC0.5 and MC1, refer to the crosslinking composition listed in the Table 1, together with their characteristic transition temperatures. For comparison, the pure uncrosslinked melt of the same main-chain polymer, studied in some detail in [24], has  $T_g \approx 38$  C and  $T_{ni} \approx 112$  C (for the longer-chain MC component).

Monodomain, aligned samples were made by preparing partially crosslinked films in a centrifuge, highly swollen in toluene (2-3 ml per 1 g of material), reacting for 25-35 minutes before evaporating the solvent and suspending the samples under load in an oven to complete the reaction for more than 5 hours at 120 C. A careful study of reaction kinetics ensured that approximately 50% of crosslinks were established in the first stage of this preparation.

When a uniaxial stress is applied to such a partially crosslinked network, the aligned monodomain state in the resulting nematic elastomer is established with the director along the stress axis. This orientation is then fixed by the subsequent second-stage reaction, when the remaining crosslinks are fully established. Following the ideas and results of [15], in all cases we performed the second-stage crosslinking in the high-temperature isotropic phase: in this way a better alignment and mechanical softness are achieved (in contrast to the crosslinking in a stretched polydomain nematic phase [15, 23], which results in a number of defects and domain walls frozen in the material).

Equilibrium transition temperatures given in the Table 1 were determined on a Perkin Elmer, Pyris 1 differential scanning calorimeter (DSC), extrapolating to low cooling rates, and the nematic phase identified by polarizing optical microscopy and X-ray scattering. Thermal expansion measurements were made by suspending the samples, without load, in a glass-fronted oven and measuring the variation in natural length of the samples with temperature,  $L(T)$ . Precise length measurements were made using a traveling microscope, as the samples were slowly cooled (at a rate  $0.5^\circ/\text{min}$ ) after the complete annealing in the isotropic state.

The force measurements were performed on a custom built device consisting of a temperature compensated stress gauge and controller (UF1 and AD20 from Pioden Controls Ltd) in a thermostatically controlled chamber (Cal 3200 from Cal Controls Ltd). The rectangular shaped samples (approximately  $30 \times 5 \times 0.3$  mm) were mounted with clamps, at room temperature, in such a way that the sample length  $L$  remains fixed throughout the experiment. The samples were then heated (at a rate  $\sim 0.5^\circ/\text{min}$ ) to the isotropic phase. The stress and temperature values were acquired by connection to a Keithley multimeter (2000 series) and stored on a PC over an IEEE interface. The increasing force was measured by the stress gauge and later correlated with the effective strain in the sample, due to the decreasing underlying natural length  $L(T)$ . Since the effective strain reached high values,  $\lambda_{\text{th}} \sim 3 - 3.5$  when  $T_{\text{ni}}$  was reached, many samples broke or tore. However, a good reproducibility of force-temperature, as well as stress-strain relations allowed one to extrapolate the data over the whole temperature range.

### 3 Thermal and mechanical equilibrium

#### Phase transitions

Figure 2 presents the data of DSC measurements of phase transformations in our materials. All samples exhibit a single nematic phase above their



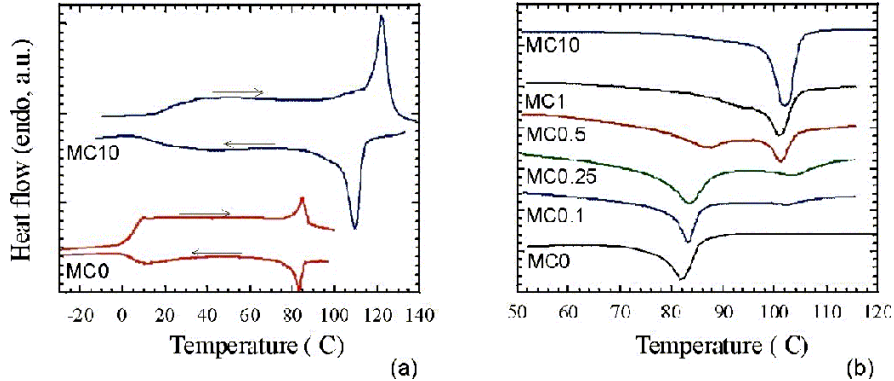


Figure 2: DSC data for the series of nematic elastomers, at 10 C/min. (a) Heating and cooling scans of MC0 and MC10, showing the glass and the nematic-isotropic transitions and their hysteresis. (b) Sequence of cooling scans of the nematic transition for all the materials in the series, MC0 to MC10 – increasing curves.

glass transition, however, the position and the morphology of phase transformations strongly depends on the composition. It is expected, and well-known, that liquid crystalline polymers show a much broader and diffuse signature of the weakly first-order nematic-isotropic transition. This effect is especially pronounced in crosslinked elastomers, where the quenched sites of random disorder introduced by crosslinks lead to a more diffuse transition and stronger hysteresis. Fig. 2(a) shows an example of heating and cooling scans for a selected sample, MC0 and MC10, at the opposite ends of the series. One can clearly recognize the effect of main-chain polymer component, which increases the glass and the nematic-isotropic transition temperatures.

Figure 2(b) focuses only on the region of nematic transition and brings together the DSC scans for all materials, obtained at the same cooling rate of 10 C/min after a long annealing at 120 C. Comparison between MC10 and MC1 tells that even at the relative proportion of MC crosslinking chains of 1% the properties of the resulting network are dominated by their effect. This observation will be supported below by the comparison of spontaneous thermal expansion of MC10 and MC1, which has the same overall character and the transition point, but rather different from the other members of the series. One should expect this, since the calculation of the relative mass of the side- and the main-chain components in our materials becomes approximately equal at the level of 1.75 mol% of MC (see Table 1).

The second key result of this DSC study, evident in all materials be-

tween MC0.1 and MC1, is the presence of two sequential nematic transitions. We have verified by X-ray and optical observations that no additional phase exists in the materials, which are optically transparent and homogeneous at all temperatures. Clearly, the higher-temperature transition is related to the main-chain nematic component of the network: its temperature hardly shifts on composition (remember that the data in Fig. 2(b) is obtained on cooling after the complete annealing), but its overall latent heat decreases in proportion with the decreasing percentage of MC. The second, lower-temperature transition is, of course, that of the side-chain polysiloxane polymer. Its temperature continuously shifts up on increasing proportion of the MC crosslinker and, accordingly, the stronger nematic field provided by the more strongly anisotropic MC polymer (which has already undergone the phase transformation, as indicated by thermal scans). We shall now investigate the related mechanical response and return to the discussion of the possible reasons for such a behavior.

## Uniaxial thermal expansion

Changing the temperature affects the nematic order parameter  $Q(T)$  of a nematic elastomer and, in a permanently aligned monodomain state, alters the effective chain anisotropy of the rubber,  $r = \ell_{\parallel}/\ell_{\perp}$ . Figure 3 shows the variation of natural length of free, unloaded samples, measured along the nematic director. Obviously, in an incompressible rubber the volume is conserved and the two perpendicular directions experience the symmetric contraction by  $1/\sqrt{\lambda}$  when the principle direction is elongated by  $\lambda = L/L_0$ . Here the length  $L(T)$  is measured with respect to the length  $L_0$  the corresponding sample has in the isotropic phase. Elongation on cooling into the nematic phase means that the network is characterised by an effective prolate anisotropy, that is  $r > 1$ , below  $T_{ni}$ . The spontaneous uniaxial thermal expansion described by the strain  $\lambda_{th}$ , Eq.(3), is an equilibrium reversible process. Fig. 3(a) illustrates this by showing the evolution of sample length for one selected material, MC0.25, on heating and on cooling. There is an evident hysteresis which, however, is rather small at the cooling rate used in this experiment. Without going into greater detail, we must mention that the characteristic response time, or equivalently – the width of hysteresis, increase dramatically with the increasing MC concentration. In the material MC0 we find no trace of a hysteresis, while in MC10 the response to changing temperature is rather slow and the hysteresis in  $L(T)$  is very noticeable at an already slow cooling/heating rate of  $0.5^{\circ}/\text{min}$ . This slow response and relaxation of main-chain nematic polymers [24], the likely reason being the freezing of chain motion in narrowly confining hairpins.

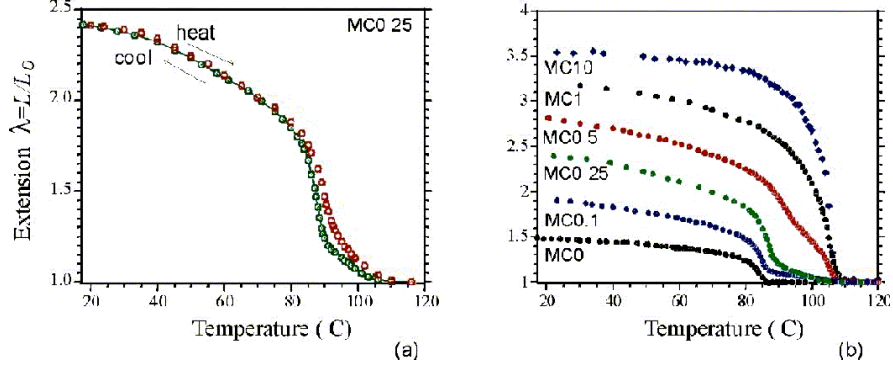


Figure 3: Uniaxial thermal expansion  $\lambda_{\text{th}} = L(T)/L_0$  for the uniaxial nematic rubber, with the temperature rate of  $\sim 0.5$  C/min. (a) Heating and cooling cycles for MC0.25, showing the effect of hysteresis. (b) Sequence of cooling cycles for all materials, from MC0 to MC10. Notice the two-stage expansion, beginning at the higher nematic transition temperature and enhanced at the lower  $T_{\text{ni}}$  – consistent with the two-transition feature of DSC data.

Analyzing the sequence of  $\lambda_{\text{th}}(T)$  data for the full series of samples, one is impressed by the high value of strain achieved, especially in the MC-containing materials. The arguments already presented above, about the relative mass of the long-chain MC material in the overall network composition becoming approximately equal to that of the siloxane side-chain polymer at the level of  $\sim \text{MC-1.75\%}$ , are confirmed by the observation that no significant further increase in the effective network anisotropy  $r = \lambda_{\text{th}}^3$  occurs in high-MC containing samples; the increase in  $\lambda_{\text{th}}$  at a given  $T$  in going from MC1 to MC10 is much less than from MC0 to MC1. One could argue that the ambient-temperature value of  $r \approx 42$  found in MC10 is close to the natural anisotropy of our MC polymer. This would make a prediction for the radius of gyration anisotropy  $R_{\parallel}/R_{\perp} \approx 6.5$  (since  $\langle R^2 \rangle \sim \ell L$ ), which is a high but not unexpected value for this type of semiflexible polymer, as seen by neutron scattering from the melt (see, e.g., [25] and references therein).

Another remarkable aspect of the results shown in the Fig. 3(b) is the dual-transition feature of the transition, similar to that seen in the DSC study. Networks with the low MC-concentration, when the main-chain component is the minority in the composition, show their first sign of nematic transition (indicated here by the initial small uniaxial expansion) at the higher  $T_{\text{ni}}$ , followed by a subsequent rapid increase at the lower  $T_{\text{ni}}$ . The amount of average network anisotropy generated at the first transition in-

creases with the concentration of MC, and is consistent with the overall latent heat of this higher-temperature transition in the Fig. 2(b). The second transition, seen as a near-critical jump in  $\lambda_{\text{th}}$  for MC0.1, moves towards higher temperatures as the MC-concentration increases, again consistently with the DSC data.

One fundamental question that arises from the results shown above is the nature of the first, higher  $T_{\text{ni}}$ , nematic transition. A natural explanation would be the phase separation of very long MC chains during the synthesis, when they are in the minority composition. It would then be natural that small volumes with the high concentration of MC undergo the nematic transition at  $\sim 108$  C. The high uniaxial elongation of these small MC-regions would, however, be absorbed by the still isotropic network of polysiloxane chains and the overall mechanical strain would be small. This would also explain the shift of the  $T_{\text{ni}}$ , because the uniaxially aligned nematic MC-regions would provide a driving field for the rest of the mesogenic material. However, it is not straightforward to reconcile this hypothesis about the phase separation with the fact that our materials show no optical inhomogeneity (which could simply mean that the MC-regions are too small), as well as with the fact that each MC-chain has to be crosslinked at both ends to a siloxane strand. Since the first-step crosslinking takes place in the presence of solvent in a well-mixed centrifuge environment, one expects a relatively homogeneous distribution of junction points, which should then be preserved after the second crosslinking stage, in spite of de-swelling. An intriguing alternative possibility could be that we observe the precursor to the nematic transition in essentially separate chains of MC. Theoretical studies [26] have long ago predicted the existence of nematic-nematic phase transition lines when two competitive ordering trends are present in the system; in that terminology, we could be observing the discontinuous  $N_{\text{III}}-N'_{\text{III}}$  transition at a temperature below  $T_{\text{ni}}$  for the change between the isotropic and the  $N_{\text{III}}$  phases. We have not pursued this question in any more depth here, instead concentrating on the mechanical aspects of nematic ordering in rubber.

## 4 Thermo-mechanical actuation

An important practical question of spontaneous thermal expansion of monodomain nematic rubbers, relevant to practical use of this effect in thermo-mechanical actuators, is the amount of stress the material can sustain. The work cycle of a corresponding artificial muscle depends on the amplitude of motion, but also on the force the nematic rubber exerts – or the load it can work under. In this section we focus on the sample MC1, which shows an

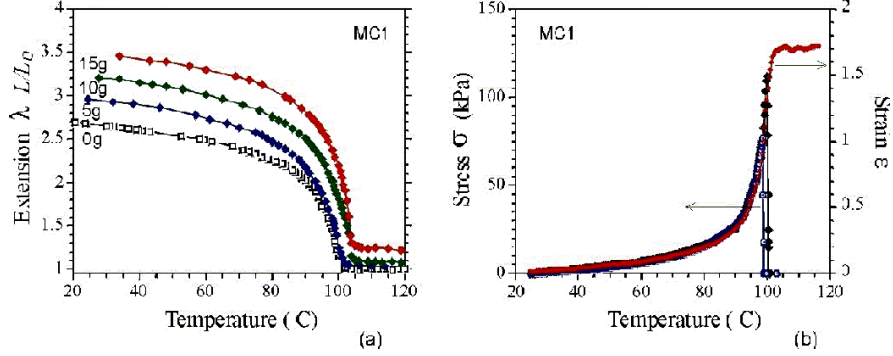


Figure 4: (a) Cooling cycles for MC1 under increasing load, corresponding to applied stress of 0, 30, 60 and 90 kPa. (b) The nominal stress exerted by a clamped strip of MC1, of fixed length  $L_{\text{fix}}$ , heated from room temperature to above  $T_{\text{ni}}$ . Symbols are the data points from different samples which were tearing at certain levels of stretching, at a stress  $\sim 100$  kPa; the solid line is the plot of underlying effective strain  $\epsilon = [L_{\text{fix}} - L(T)]/L(T)$  (values on the second  $y$ -axis).

almost maximal strain  $\lambda_{\text{th}}(T)$ , but still has a reasonably fast response and small hysteresis.

Figure 4(a) shows the difference in thermal expansion curves when the sample was loaded with increasing weights. For the sample of cross-section area  $\sim 1.5 \text{ mm}^2$  each 5 g of weight corresponds to the stress  $\sigma \approx 30$  kPa; the curves in the plot are for the stress increasing from 0 to 90 kPa. Clearly, the qualitative nature of the effect is preserved when changing the temperature under load. An increase in the strain values is the natural consequence of rubber elasticity: at any given temperature and natural length, the applied load would cause an extra stretching of the rubber band. Several interesting effects are seen in this plot, in particular, the small but unambiguous shift of the nematic transition temperature,  $\Delta T_{\text{ni}} \sim 5^\circ$ , with increasing load. Such an effect is expected on theoretical grounds in a weak first-order transition system in an external field – however, in ordinary liquid crystals, electric and magnetic fields are usually too small to create a noticeable shift. On the other hand, there is no trace of supercritical behaviour or paranematics phase above  $T_{\text{ni}}$  [27]: the transition remains abrupt and well-defined; the small increase of  $\lambda$  above  $T_{\text{ni}}$  is purely due to the rubber-elastic response to the applied load.

Another practically important experiment is reported in Fig. 4(b). Here

we measure the force that a nematic rubber band can exert when thermally contracting. A strip of MC1 elastomer with a cross-section of  $5 \times 0.3$  mm (standard in all experiments described in this paper) is rigidly clamped in a dynamometer device at ambient temperature, so that its length  $L$  remains constant. On heating, the underlying natural length decreases,  $L_0(T)$ , according to the data of the previous section, cf. Fig. 3(b) for MC1. Accordingly, the effective extensional strain increases in the material and the sample exerts an increasing force on its clamped ends. This force is measured and transformed into the nominal stress by dividing by the sample cross-section area.

The plot in Fig. 4(b) shows two separate experiments on heating the constrained rubber band MC1, circles and diamonds data points (the reproducibility of results is comforting). In both cases the sample broke before reaching the isotropic phase – clearly, the stress of the order of 100 kPa has been the limit this particular material could bear (one could conceivably increase the strength by tailoring the sample shape and in particular, its thickness). We performed a number of such measurements and the results are very reproducible for a given material and sample shape. The second  $y$ -axis on this plot gives the variation of the underlying effective strain. We calculate it determining the actual gradient of underlying displacement with respect to the “virtual” equilibrium length,  $\varepsilon = [L_{\text{fix}} - L(T)]/L(T)$ , where  $L_{\text{fix}}$  is device-fixed, while  $L(T)$  follows the data measured and reported in the previous section. One can clearly see that the internal stress and the effective strain follow exactly the same graph and, therefore, are linear functions of each other over a large region of deformations.

## 5 Conclusions

In this article we report the systematic study of uniaxial thermal expansion of monodomain nematic elastomers. Composite materials combined main-chain and side-chain nematic polymers in their networks and the results are sensitive functions of concentration of the MC component. Increasing the proportion of MC in the otherwise side-chain nematic network has a great effect on the average effective anisotropy of polymer chains and, as a result, on the magnitude of spontaneous strain  $\lambda_{\text{th}}$ . At the same time, there is a pronounced slowing down of all response processes: the stress relaxation, the equilibration of natural length and the shape recovery. One does expect such slow dynamics in MC-dominated materials, which is consistent with other studies of main-chain nematic polymers. The isotropic-nematic transition at  $T_{\text{ni}}$  is abrupt in all our materials, with no supercritical effects or parane-

matic phase. However, both the mechanical and the thermal data indicate that at a small concentration of MC, the network experiences a sequence of two nematic transitions. A possible explanation for this effect could be a microphase separation of MC-rich regions, however, there factors against it and the question is far from being fully understood.

The study of mechanical actuation, that is the contraction under load, or exerting a force on changing the temperature shows that uniformly aligned nematic elastomers have a great potential in practical applications, from stress and deformation gauges, to artificial muscles and micromanipulators. On the map of material properties of different materials used in actuator design [28], the nematic elastomers would occupy the region of low stress (unlikely to exceed a few MPa) and extremely high deformations. In comparison, the present “large-amplitude” actuators are based on shape-memory alloys, which reach strains of up to 10% – something that pales in comparison with over-300% deformations described in this work.

## Acknowledgements

This work has been supported by EPSRC UK. We are grateful to S.M. Clarke, M. Warner and A. Hotta for a number of useful discussions and help with the measurements. Special thanks to H. Finkelmann and A. Greve for advice and help with material synthesis procedures.

## References

- [1] W. Gleim and H. Finkelmann, in: *Side-Chain Liquid Crystal Polymers*, ed. C. B. McArdle (Blackie & Sons, 1989) p.287.
- [2] G. G. Barclay and C. K. Ober, *Progr. Polym. Sci.* **18** 899 (1993).
- [3] M. Warner and E. M. Terentjev, *Prog. Polym. Sci.*, **21**, 853 (1996).
- [4] H. R. Brand and H. Finkelmann, in: *Handbook of Liquid Crystals*, ed D. Demus et al. (Wiley-VCH, Weinheim, 1998), Vol.3, Chapter V.
- [5] E. M. Terentjev, *J. Phys. Cond. Mat.*, **11**, R239 (1999).
- [6] H. Finkelmann, E. Nishikawa, G. G. Pereira and M. Warner, *Phys. Rev. Lett.* – to appear
- [7] G. R. Mitchell, F. J. Davis and W. Guo, *Phys. Rev. Lett.* **71** 2947 (1993).
- [8] H. Finkelmann, I. Kundler, E. M. Terentjev and M. Warner, *J. Physique II*, **7**, 1059, (1997).
- [9] C.-C. Chang, L.-C. Chien and R. B. Meyer, *Phys. Rev. E* **56**, 595 (1997).
- [10] E. M. Terentjev, M. Warner, R. B. Meyer and J. Yamamoto, *Phys. Rev. E* **60**, 1872, (1999).
- [11] S. M. Clarke, A. R. Tajbakhsh, E. M. Terentjev and M. Warner, *Phys. Rev. Lett.* **86**, 4044 (2001).
- [12] S. M. Clarke, A. R. Tajbakhsh, E. M. Terentjev, C. Remillat, G. R. Tomlinson and J. House, *J. Appl. Phys.* **89**, 6530 (2001).
- [13] S. Kutter and E. M. Terentjev, *Euro. Phys. J. B* – to appear (cond-mat/0106193).
- [14] L. Fetters, D. Lohse, D. Richter, T. Witten and A. Zirkel, *Macromolecules*, **27**, 4639 (1994).
- [15] J. Küpfer and H. Finkelmann, *Macromol. Rapid Comm.* **12**, 717 (1991).
- [16] J. Schätzle, W. Kaufhold and H. Finkelmann, *Makromol. Chem.* **190**, 3269 (1989).
- [17] N. Assfalg and H. Finkelmann, *Kaut. Gummi. Kunstst.* **52**, 677 (1999).



- [18] G. H. F. Bergmann, H. Finkelmann, V. Percec, and M. Zhao, *Macromol. Rapid. Comm.* **18**, 353 (1997).
- [19] M. Warner and X. J. Wang, *Macromolecules* **24**, 4932 (1991).
- [20] P. G. de Gennes, M. Hebert and R. Kant, *Macromol. Symp.* **113**, 39 (1997).
- [21] H. Finkelmann, A. Greve and M. Warner, *Euro. Phys. J. E* **5**, 281 (2001).
- [22] V. Percec, M. Kawasumi, *Macromolecules*, **24**, 6318 (1991).
- [23] S. V. Fridrikh and E. M. Terentjev, *Phys. Rev. E* **60**, 1847, 1999.
- [24] F. Elias, S. M. Clarke, R. Peck and E. M. Terentjev, *Europhys. Lett.* **47**, 442, (1999).
- [25] M. H. Li, A. Brulet, P. Davidson, P. Keller, J. P. Cotton, *Phys. Rev. Lett.* **70**, 2297 (1993).
- [26] W. Renz and M. Warner, *Proc. Roy. Soc. Lond. A Mat* **417**, 213 (1988).
- [27] S. Disch, C. Schmidt and H. Finkelmann, *Macromol. Rapid Comm.* **15**, 303 (1994).
- [28] M. F. Ashby, *Materials Selection and Process in Mechanical Design*. (Butterworth Heinemann, Oxford, 1999).

This figure "chem.jpg" is available in "jpg" format from:

<http://arxiv.org/ps/cond-mat/0106138v3>

This figure "dsc.jpg" is available in "jpg" format from:

<http://arxiv.org/ps/cond-mat/0106138v3>

This figure "load.jpg" is available in "jpg" format from:

<http://arxiv.org/ps/cond-mat/0106138v3>

This figure "therm.jpg" is available in "jpg" format from:

<http://arxiv.org/ps/cond-mat/0106138v3>